Proceedings of the ASME 2020
Dynamic Systems and Control Conference
DSCC2020
October 5-7, 2020, Virtual, Online

DSCC2020-3127

MODELING ANALYSIS OF THE WRIST DYNAMICS VIA AN ELLIPSOIDAL JOINT

Jiamin Wang, Sunit K. Gupta , Oumar Barry*
Department of Mechanical Engineering
Virginia Polytechnic Institute and State University
Blacksburg, Virginia 24061

ABSTRACT

An accurate wrist model is crucial to the understanding of human wrist mechanics and the development of forearm rehabilitation devices. This paper studied the nonlinear dynamics of the wrist through an ellipsoidal joint model. Compared to many studies where a universal joint is used to model the wrist, the proposed ellipsoidal model intends to better approximate the human wrist biomechanics with the use of kinematic constraints. The constraint on the original 3-dimensional rotation of the wrist is realized based on a quaternion formulation, reducing the wrist kinematics to the coupled 2-degree-of-freedom motions of flexion-extension and radial-ulnar deviation. The ellipsoidal joint also introduces additional coupling from the translational motion constraints. The multibody modeling of the wrist model is then established. The stability and control of the model are analyzed based on a constrained state-space model. Numerical simulations validate the analytical results and demonstrate the coupled dynamical behavior of the wrist. The simulations also show that the proposed model constraint is an ideal base regression function for wrist joint parameter identification. Finally, with the involvement of nonlinear stiffness and damping, chaotic-like behaviors and limit cycles are observed. The approach in this study is also generally applicable to a family of ellipsoidal joint systems.

NOMENCLATURE

The mathematical notations used are listed as following:

$\|\mathbf{Z}\|_n$ The induced n-norm of a matrix $\mathbf{Z}$ ($n = 2$ if not specified)

$\mathbf{z}_1 \times \mathbf{z}_2$ Multiplications of quaternions $\mathbf{z}_1$ (4×1) and $\mathbf{z}_2$ (4×1)

$\bar{\mathbf{z}}$ Conjugation of quaternion $\mathbf{z}$ (4×1)

$\mathbf{z}_{m\times n}$ A $m\times n$ matrix with all elements as $\mathbf{z}\in\mathbb{R}$ (fits along with its neighboring blocks if no dimension specified)

$\mathbf{I}_n$ Identity matrix of a specific dimension n (fits along with its neighboring blocks if no dimension specified)

$\mathbf{Z}^{-T}$ The transposed inverse of $\mathbf{Z}$ (since $(\mathbf{Z}^{-1})^{\mathrm{T}} = (\mathbf{Z}^{\mathrm{T}})^{-1}$)

$\mathbf{Z}^{+}$ The Moore-Penrose pseudo inverse of $\mathbf{Z}$

$\mathbf{Z} > 0$ A square matrix $\mathbf{Z}$ is positive definite

$\mathbf{Z}^m$ Raises each element of matrix $\mathbf{Z}$ to the power of m

$\mathrm{diag}([\mathbf{z}])$ Convert a m-dimensional vector $\mathbf{z}$ into a $m\times m$ diagonal matrix with elements from $\mathbf{z}$

1 Introduction

The wrist joint is pivotal to human in performing manipulation tasks. A better understanding of the wrist biomechanics is beneficial to developing rehabilitation treatments (i.e., therapy, device) [1] for patients undergoing recovery from injuries and neurological diseases (e.g., stroke [2, 3], Parkinson's Disease, Essential Tremor [4–7]). The wrist joint is a highly coupled multiple degree-of-freedom (DOF) biomechanism, whose principle motions can be generalized as flexion-extension (FE) and radial-ulnar deviation (RUD) [8, 9]. The approximate rotation axes of the FE and RUD motions are shown in Fig. 1. The biomechanics of the wrist has been extensively investigated, which includes the modeling of the wrist kinematics from experimental data [9, 10], coupling between the wrist motion [11], the stiffness and damping of wrist [12, 13].

The musculoskeletal anatomy of the wrist is presented in Fig. 2. In Fig. 2(a), The radiocarpal (RC) joint is located between the radial-ulnar row and the proximal row (highlighted in blue), which is a ellipsoidal/condyloid joint that possesses two primary DOFs. The midcarpal (MC) joint located between

*Corresponding Author (Email: obarry@vt.edu)

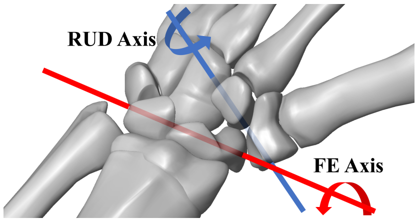

FIGURE 1: The approximate location of RUD and FE rotational axes of the wrist on a left forearm [8]

the proximal (highlighted in red) and distal row is also approximately ellipsoidal. However, in many studies, the kinematics of the wrist joint is approximated by one or multiple universal joints, where the wrist motions take place in sequence [10–12, 14, 15]. From Fig. 2(b), it is shown that the actuation of the wrist joint is contributed by different muscle combinations. Unlike the universal joints, there is no mechanical axes for the FE and RUD motion. It should also be noted that the model can be uniquely defined by the sequence of the rotational motions. For example, the first-FE-then-RUD model [11, 15] is different from the first-RUD-then-FE model [16]. Finally, the coupled translational motions at the wrist were inaccurately simplified as fixed points in many models, which did not take the geometric constraints into consideration. [17].

In this paper, a novel ellipsoidal joint model for the wrist is proposed. Unlike the previous universal joint models, the wrist is first modeled as a 3-DOF rotary joint. A quaternion based constraint is then applied to the model, reducing it to the FE

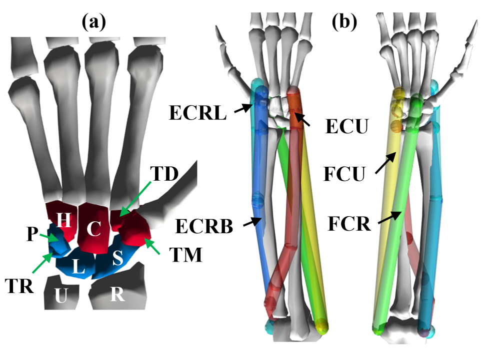

FIGURE 2: 3D model of the wrist musculoskeletal anatomy acquired from OpenSim [15]. (a) shows the radial (R) bone, the ulnar (U) bone, the proximal carpal bones (blue): S - Scaphoid, L - Lunate, TR - Triquetrum, P - Pisiform; and the distal carpal bones (red): TM - Trapezium, TD - Trapezoid, C - Capitate, H - Hamate. (b) illustrates the muscles that actuates the wrist joints: ECRB - Extensor Carpi Radialis Brevis, ECRL - Extensor Carpi Radialis Longus, ECU - Extensor Carpi Ulnaris, FCU - Flexor Carpi Ulnaris, FCR - Flexor Carpi Radialis. Wrist motions are acutated by: (1) flexion: FCR and FCU; (2) extension: ECRB, ECRL and ECU; (3) radial deviation: ECRB, ECRL and FCR; and (4) ulnar deviation: FCU and ECU.

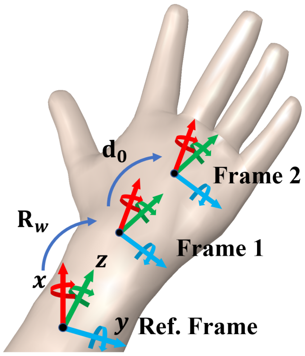

FIGURE 3: A right human forearm located in a fixed Cartesian coordinate frame.

and RUD motion. Coupling from translational motion is also introduce based on the properties of ellipsoidal joint. The model avoids the uniqueness of sequenced rotation models, making it a general model structure for regression and dynamical analysis.

The rest of the paper is arranged as follows. In Section 2 the kinematics of the proposed wrist joint model and its relationship to the existing sequenced rotation models are explained. In Section 3, the dynamical model of the wrist is established along with the analysis of its equilibrium and stability. Numerical simulation is carried out in Section 4 to validate the analytical result and demonstrate the dynamical behavior of the wrist model. Finally, Section 5 summarizes the findings and leads to the future work.

2 The Kinematics of Ellipsoidal Joint Model

A right human forearm is presented in Fig. 3. With respect to the fixed reference frame, FE is defined along y direction, RUD is defined along x direction, and z direction is the pronation-supination (PS) direction. As the wrist rotates, the orientation of the hand with respect to the forearm can always be presented by a 3×3 rotation matrix. The rotation matrix can be formulated by Euler Angles, i.e., the yaw-pitch-roll (z-y-x) formulation of the rotation matrix is

$$\mathbf{R}_w(\mathbf{z}_\theta) = \mathbf{R}_z(\theta_z)\mathbf{R}_y(\theta_y)\mathbf{R}_x(\theta_x) \tag{1}$$

where $\mathbf{z}_\theta = [\theta_x,\ \theta_y,\ \theta_z]^\mathrm{T}$ is the measurement of the wrist rotation, and $\mathbf{R}_x$, $\mathbf{R}_y$, and $\mathbf{R}_z$ are respectively the rotational matrices around x, y, and z axis. In the universal joint wrist models, it is assumed that $\theta_z \approx 0$. Here, the generalized coordinate for FE and RUD motions is defined as $\mathbf{q}_w = [q_1,\ q_2]^\mathrm{T}$, where $q_1 > 0$ is extension, $q_1 < 0$ is flexion, $q_2 > 0$ is radial deviation, and $q_2 < 0$ is ulnar deviation. Therefore, the rotational matrix can also be obtained as

$$\mathbf{R}_{w,1}(\mathbf{q}_w) = \mathbf{R}_w = \mathbf{R}_y(q_1)\mathbf{R}_x(q_2) \tag{2}$$

which is the first-FE-then-RUD sequenced rotation. In other models, the first-RUD-then-FE sequenced rotation is adopted as

$$\mathbf{R}_{w,2}(\mathbf{q}_w) = \mathbf{R}_w = \mathbf{R}_x(q_2)\mathbf{R}_y(q_1) \tag{3}$$

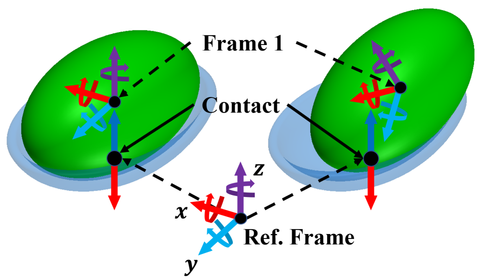

FIGURE 4: Illustration of an ellipsoidal joint [17], where the blue and red vectors at the contact points are respectively normal to the green oval surface and the blue cavity surface.

where the rotation sequence has been reverted. Some models also adopted two serially connected universal joint models that respectively represent the radiocarpal and midcarpal motions [14, 15]. An example of this can be written as

$$\mathbf{R}_{w,3}(\mathbf{q}_w) = \mathbf{R}_w = \mathbf{R}_y(q_1/2)\mathbf{R}_x(q_2/2)\mathbf{R}_y(q_1/2)\mathbf{R}_x(q_2/2) \quad (4)$$

Note that given a 3D displacement $\mathbf{d}$ in the rotated frame, the above rotation matrices will result in distinctive $\mathbf{R}_{w,i}\mathbf{d}$ $(i = 1,2,3)$ due to the uniqueness of sequenced rotation. This has led to the exploration of a more general wrist kinematic model.

2.1 Quaternion Based Constraint on Wrist Rotation

An ellipsoidal joint is illustrated in Fig. 4 [17], which is similar to a ball joint except that the cavity prevents the spinning motion around z axis. In the wrist, the PS motion is largely constrained. The proposed rotation model is constructed based on the rotation matrix $\mathbf{R}_w$ in Eq.(1). A constraint can be introduced onto $\mathbf{z}_\theta$ as

$$\begin{aligned} r_{\mathbf{z}_\theta}(\mathbf{z}_\theta) = &\ \left[1\ \mathbf{0}_{1\times3}\right] \left(\left[\mathbf{0}_{1\times3}\ 1\right]^{\mathrm{T}} \times (\bar{\mathbf{p}}_0 \times \mathbf{p}(\mathbf{z}_\theta))\right) \\ = &\ \cos(\theta_z/2)\sin(\theta_x/2)\sin(\theta_y/2) \\ &-\cos(\theta_x/2)\cos(\theta_y/2)\sin(\theta_z/2) \\ = &\ 0 \end{aligned} \quad (5)$$

where $\mathbf{p}$ is the quaternion that represents the rotation $\mathbf{R}_w$ (note that $\mathbf{R}_w$ is independent of $\mathbf{z}_\theta$), $\mathbf{p}_0$ is quaternion of an arbitrary fixed frame, which is set as $\mathbf{p}_0 = [1,\ \mathbf{0}_{1\times3}]^{\mathrm{T}}$ in this study. As a result, $r_{\mathbf{z}_\theta,1}$ can be interpreted as: the rotation $\mathbf{p}$ is constrained on the z direction of the coordinate frame defined by the orientation $\mathbf{p}_0$. It should be noted that in this constraint, θ_z is not set to zero due to the coupling between q_1 and q_2. This indicate that the proposed model does not assume the FE and RUD motions as orthogonal [18, 19]. However, the rotation axis (imaginary part) of $\mathbf{p}$ does not contain the z component.

The relationship between the proposed model and the existing models can also be explained by the quaternion constraint. By measuring $\mathbf{z}_\theta$ (here $\mathbf{z}_\theta$ is not selected as $\mathbf{q}_w$), the constraint for $\mathbf{R}_{w,1}$ can be redesigned as

$$r_{\mathbf{z}_\theta,1}(\mathbf{z}_\theta, \mathbf{q}_w) = r_{\mathbf{z}_\theta} - \sin(q_1/2)\sin(q_2/2) = 0 \quad (6)$$

for $\mathbf{R}_{w,2}$, the constraint can be written as

$$r_{\mathbf{z}_\theta,2}(\mathbf{z}_\theta, \mathbf{q}_w) = r_{\mathbf{z}_\theta} + \sin(q_1/2)\sin(q_2/2) = 0 \quad (7)$$

and for $\mathbf{R}_{w,3}$, the constraint is

$$r_{\mathbf{z}_\theta,3}(\mathbf{z}_\theta, \mathbf{q}_w) = r_{\mathbf{z}_\theta} - \sin(q_1/2)\sin(q_2/2)/2 = 0 \quad (8)$$

From these equations, it is interesting to notice that the proposed model is the intermediate of $\mathbf{R}_{w,1}$ and $\mathbf{R}_{w,2}$. Also, $\mathbf{R}_{w,3}$ is more similar to the proposed model than $\mathbf{R}_{w,1}$. All of these models have similar results when the FE and RUD angle are small. In summary, by using the constraint in Eq.(5), the effect of rotation sequence is avoided while Euler Angle measurements can still be used to quantify the degree of FE and RUD. Even if the wrist joint behave like a universal joint, Eq.(6) and (7) can be used to identify the rotation sequence of the universal joint.

2.2 Translational Constraints in the Wrist

Translational displacement of a point on the hand during wrist motion is not simply affected by R_w. As pointed out in Fig. 4, unlike a ball joint, the cavity and the oval shape are not always concentric. By defining the contact point as the origin of the fixed reference frame and the center of the oval shape as the origin of the rotated frame (Frame 1), the contact point on the oval surface satisfy the ellipsoidal equation constraint

$$r_{d,1}(\mathbf{z}_\theta, \mathbf{q}_d) = \mathbf{q}_d^{\mathrm{T}}\mathbf{R}_w \mathrm{diag}(\left[c_a^2\ c_b^2\ c_c^2\right])^{-1}\mathbf{R}_w^{\mathrm{T}}\mathbf{q}_d - 1 = 0 \quad (9)$$

where $\mathbf{q}_d = [q_x,\ q_y,\ q_z]^{\mathrm{T}}$ is the generalized coordinate of the center of the oval shape in the fixed frame, and c_a, c_b, c_c are the radius parameters of the ellipsoid. In this study, it is also assumed that the oval shape created by the carpal bones will slide back into the cavity formed by the radial and ulnar bones. Thus, the normal vector of the oval surface at the contact point is also normal to the cavity surface. The normal vector to the ellipsoidal surface in Frame 1 can be calculated as

$$\mathbf{v}_n = 2\ \mathrm{diag}(\left[c_a^2\ c_b^2\ c_c^2\right])^{-1}\mathbf{R}_w^{\mathrm{T}}\mathbf{q}_d \quad (10)$$

Therefore, the second set of translational constraints can be formed as

$$\mathbf{r}_{d,2}(\mathbf{q}_d, \mathbf{z}_\theta) = \left[\mathbf{I}_2\ \mathbf{0}_{2\times1}\right]\mathbf{R}_w\mathbf{v}_n = 0 \quad (11)$$

which fixes the normal vector of the ellipsoidal surface at the contact point with the z axis in the fixed frame [17].

By combining all the constraints together as

$$\mathbf{r} = \left[r_\theta\ r_{d,1}\ \mathbf{r}_{d,2}^{\mathrm{T}}\right]^{\mathrm{T}} = \mathbf{0}_{4\times1} \quad (12)$$

the constraints Jacobian $\mathbf{J}_r$ can be calculated from the derivative of $\mathbf{r}$ as

$$\dot{\mathbf{r}} = \mathbf{J}_r\left[\dot{\mathbf{z}}_\theta^T\ \dot{\mathbf{q}}_d^T\right]^{\mathrm{T}} = 0 \quad (13)$$

Here, by selecting generalized coordinate $\mathbf{q}_w$ as $\mathbf{q}_w = [q_1,\ q_2]^{\mathrm{T}} = [\theta_y,\ \theta_x]^{\mathrm{T}}$, we obtain

$$\dot{\mathbf{q}}_r = \left[\dot{\theta}_z^T\ \dot{\mathbf{q}}_d^T\right]^{\mathrm{T}} = -\mathbf{J}_{r,2}^{-1}\mathbf{J}_{r,1}\dot{\mathbf{q}}_w \quad (14)$$

with

$$\mathbf{J}_r = \begin{bmatrix}\mathbf{J}_{r,1} \ \mathbf{J}_{r,2}\end{bmatrix} \tag{15}$$

where $\mathbf{J}_{r,1}$ is the 4×2 Jacobian matrix corresponding to $\mathbf{q}_w$, and $\mathbf{J}_{r,2}$ is the one for the remaining terms. Equation (14) will be used to form the minimal-order state-space model used for analysis in the upcoming sections.

3 Dynamical Modeling and Analysis

This section introduces the dynamic modeling of the forearm based on the proposed wrist kinematic model. As mentioned previously, the fixed reference frame is located at the contact point, which will also be selected as the global frame for the modeling. The inertial frame (Frame 2 in Fig. 3) of the wrist is translationally displaced by $\mathbf{d}_0$ from the rotated frame located at the center of the oval shape. Therefore, by setting $\mathbf{q}_0 = [\mathbf{z}_\theta^T,\ \mathbf{q}_d^T]^\mathrm{T}$, the absolute translational position and velocity of the inertial frame is

$$\mathbf{d}_m = \mathbf{R}_w\mathbf{d}_0 + \mathbf{q}_d; \quad \dot{\mathbf{d}}_m = \mathbf{J}_d\dot{\mathbf{q}}_0 \tag{16}$$

Provided that the angular velocity of the body (in Frame 2) is

$$\omega = \begin{bmatrix}\omega_x \ \omega_y \ \omega_z\end{bmatrix}^\mathrm{T} = \mathbf{J}_\omega\dot{\mathbf{q}}_0 \tag{17}$$

the inertia matrix $\mathbf{M}_0(\mathbf{q}_0)$ can be calculated as

$$\mathbf{M}_0 = \begin{bmatrix}\mathbf{J}_\omega^\mathrm{T} \ \mathbf{J}_d^\mathrm{T}\end{bmatrix}\begin{bmatrix}\Phi & \mathbf{0}_{3\times3}\\ \mathbf{0}_{3\times3} & m\mathbf{I}_3\end{bmatrix}\begin{bmatrix}\mathbf{J}_\omega\\ \mathbf{J}_d\end{bmatrix} \tag{18}$$

and the Coriolis and centripetal force matrix $\mathbf{C}_0(\mathbf{q}_0,\dot{\mathbf{q}}_0)$ can be calculated as

$$s(\omega) = \mathrm{skew}(\omega) = \begin{bmatrix}0 & -\omega_z & \omega_y\\ \omega_z & 0 & -\omega_x\\ -\omega_y & \omega_x & 0\end{bmatrix};$$
$$\mathbf{C}_0 = \begin{bmatrix}\mathbf{J}_\omega^\mathrm{T} \ \mathbf{J}_d^\mathrm{T}\end{bmatrix}\begin{bmatrix}\Phi & \mathbf{0}_{3\times3}\\ \mathbf{0}_{3\times3} & m\mathbf{I}_3\end{bmatrix}\begin{bmatrix}\dot{\mathbf{J}}_\omega\\ \dot{\mathbf{J}}_d\end{bmatrix} - \mathbf{J}_\omega^\mathrm{T}s(\Phi\omega)\mathbf{J}_\omega \tag{19}$$

where m and Φ are the mass and the 3×3 rotational inertia matrix, respectively. Based on this setup, the unconstrained dynamical model can be established as

$$\mathbf{M}_0(\mathbf{q}_0)\ddot{\mathbf{q}}_0 = -\mathbf{C}_0(\mathbf{q}_0,\dot{\mathbf{q}}_0)\dot{\mathbf{q}}_0 + \mathbf{J}_{u,0}(\mathbf{q}_0)^\mathrm{T}\mathbf{u}_0 \tag{20}$$

In this formulation, the stiffness, damping, and other terms are assumed to come from the external input, which can be provided by the muscles.

The minimal-order state-space model can be formulated simply by having

$$\dot{\mathbf{q}}_0 = \mathbf{J}_{r,w}\dot{\mathbf{q}}_w = \begin{bmatrix}\mathbf{I}_2\\ -\mathbf{J}_{r,2}^{-1}\mathbf{J}_{r,1}\end{bmatrix}\begin{bmatrix}0 & 1\\ 1 & 0\end{bmatrix}\dot{\mathbf{q}}_w \tag{21}$$

which leads to

$$\mathbf{M} = \mathbf{J}_{r,w}^\mathrm{T}\mathbf{M}_0\mathbf{J}_{r,w}; \quad \mathbf{C} = \mathbf{J}_{r,w}^\mathrm{T}\mathbf{C}_0\mathbf{J}_{r,w} - \mathbf{J}_{r,w}^\mathrm{T}\mathbf{M}_0\dot{\mathbf{J}}_{r,w}; \quad \mathbf{J}_u = \mathbf{J}_{u,0}\mathbf{J}_{r,w}$$
$$\mathbf{M}\ddot{\mathbf{q}}_w = -\mathbf{C}\dot{\mathbf{q}}_w + \mathbf{J}_u\mathbf{u}_0; \quad \dot{\mathbf{q}}_r = -\mathbf{J}_{r,2}^{-1}\mathbf{J}_{r,1}\dot{\mathbf{q}}_w \tag{22}$$

where $\dot{\mathbf{q}}_r$ can be considered as the nonholonomic state of the system. The state-space form of the system can be written as

$$\mathbf{x} = \begin{bmatrix}\mathbf{q}_0^\mathrm{T} \ \dot{\mathbf{q}}_w^\mathrm{T}\end{bmatrix}^\mathrm{T}$$
$$\dot{\mathbf{x}} = f(\mathbf{x},\mathbf{u}_0) = \begin{bmatrix}\mathbf{J}_{r,w}\dot{\mathbf{q}}_w\\ -\mathbf{M}^{-1}\mathbf{C}\dot{\mathbf{q}}_w + \mathbf{M}^{-1}\mathbf{J}_u^\mathrm{T}\mathbf{u}_0\end{bmatrix} \tag{23}$$

The expression of Eq.(23) is too complicated to be presented. For the convenience of analysis, a set of simplified system parameters $\mathbf{c} = [c_0,\ k_c,\ l_0,\ \phi_0,\ k_\phi]$ is then selected to replace the original system parameters

$$c_a = c_c = c_0; \quad c_b = k_c c_0;$$
$$\mathbf{d}_0 = \begin{bmatrix}0 \ 0 \ l_0\end{bmatrix}^\mathrm{T}; \quad \Phi = \mathrm{diag}(\begin{bmatrix}\phi_0 \ \phi_0 \ k_\phi\phi_0\end{bmatrix}) \tag{24}$$

The input u_0 and its Jacobian $J_{u,0}$ are designed as

$$\mathbf{u}_0 = -\mathbf{K}_p\varepsilon_w - \mathbf{K}_d\dot{\varepsilon}_w + \mathbf{u}_c; \quad J_{u,0} = \begin{bmatrix}\begin{bmatrix}0 & 1\\ 1 & 0\end{bmatrix} & \mathbf{0}_{2\times4}\end{bmatrix}^\mathrm{T} \tag{25}$$

where $\mathbf{K}_p,\ \mathbf{K}_d > 0$ are respectively the proportional and derivative control gain matrices; $\mathbf{u}_c$ is the additional control input; and the error ε is defined as

$$\varepsilon_w = \begin{bmatrix}\varepsilon_1 \ \varepsilon_2\end{bmatrix}^\mathrm{T} = (\mathbf{q}_w - \rho) = (\mathbf{q}_w - \begin{bmatrix}\rho_1 \ \rho_2\end{bmatrix}^\mathrm{T}) \tag{26}$$

with ρ as the reference. Note that the stiffness and damping matrices are not necessarily diagonal or symmetric, as it is pointed out by studies that shows the principle components of the wrist stiffness are not necessarily along the FE and RUD axes [20]. Therefore, when $\mathbf{u}_c = \mathbf{0}$ and $|\theta_x|,\ |\theta_y|,\ |\theta_z| < \pi/2$, the equilibrium $\mathbf{x}_0$ of the minimal state-space system that satisfies the constraint $\mathbf{r}$ can be obtained as

$$\mathbf{z}_{\theta,0} = \begin{bmatrix}\rho_2 \ \rho_1 \ \theta_{z,0}\end{bmatrix}^\mathrm{T}; \quad \mathbf{q}_{d,0} = \begin{bmatrix}c_{d,x}/c_{d,0} \ c_{d,y}/c_{d,0} \ c_{d,z}\end{bmatrix}^\mathrm{T}$$
$$\mathbf{x}_0 = \begin{bmatrix}\mathbf{z}_{\theta,0}^\mathrm{T} \ \mathbf{q}_{d,0}^\mathrm{T} \ \mathbf{0}_{1\times2}\end{bmatrix}^\mathrm{T} \tag{27}$$

where

$$\begin{aligned}
\theta_{z,0} &= 2\arctan(\sin(\rho_1/2)\sin(\rho_2/2)/\cos(\rho_1/2)\cos(\rho_2/2))\\
c_{d,0} &=(-k_c^2\cos(\rho_2)^2\cos(\rho_1)^2 + k_c^2\cos(\rho_1)^2\\
&\quad + \cos(\rho_2)^2\cos(\rho_1)^2 - \cos(\rho_1)^2 + 1)^{1/2}\\
c_{d,x} &= -\,(c_0\cos(\rho_1)(k_c^2-1)(\cos(\theta_{z,0})\sin(\rho_1)\cos(\rho_2)^2\\
&\quad + \sin(\rho_2)\sin(\theta_{z,0})\cos(\rho_2) - \cos(\theta_{z,0})\sin(\rho_1)))\\
c_{d,y} &=(c_0\cos(\rho_1)(k_c^2-1)(\cos(\theta_{z,0})\sin(\rho_2)\cos(\rho_2)\\
&\quad - \sin(\rho_1)\sin(\theta_{z,0})\cos(\rho_2)^2 + \sin(\theta_{z,0})\sin(\rho_1)))\\
c_{d,z} &=c_0(k_c^2\sin(\rho_2)^2 - k_c^2\sin(\rho_2)^2\sin(\rho_1)^2\\
&\quad + \sin(\rho_2)^2\sin(\rho_1)^2 - \sin(\rho_2)^2 + 1)^{1/2}
\end{aligned} \tag{28}$$

The stability of the system at the fixed point is guaranteed for $|\theta_x|,\ |\theta_y|,\ |\theta_z| < \pi/2$ and any symmetric $\mathbf{K}_p, \mathbf{K}_d > 0$. By constructing the Lyapunov Function V as

$$V = 0.5\dot{\varepsilon}_w^\mathrm{T}\mathbf{M}\dot{\varepsilon}_w + 0.5\varepsilon_w^\mathrm{T}\mathbf{K}_p\varepsilon_w \tag{29}$$

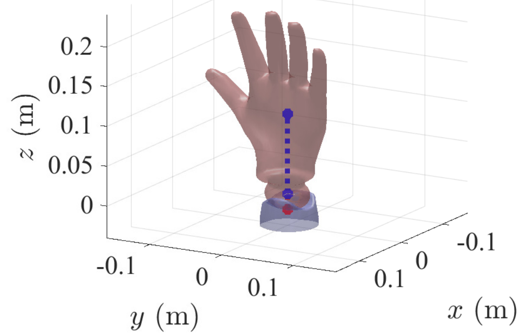

FIGURE 5: The 3D model of the wrist joint model in the MATLAB simulation. The red line indicate the displacement between the Ref. Frame and Frame 1, and the blue line shows the displacement between Frame 1 and Frame 2.

the derivative of V is obtained as

$$\begin{aligned}\dot{V} &= 0.5\dot{\varepsilon}_w^{\mathrm{T}}\dot{\mathbf{M}}\dot{\varepsilon}_w + \dot{\varepsilon}_w^{\mathrm{T}}\mathbf{M}\ddot{\varepsilon}_w + \varepsilon_w^{\mathrm{T}}\mathbf{K}_p\dot{\varepsilon}_w \\ &= 0.5\dot{\varepsilon}_w^{\mathrm{T}}\dot{\mathbf{M}}\dot{\varepsilon}_w - \dot{\varepsilon}_w^{\mathrm{T}}(-\mathbf{M}\ddot{\rho} + \mathbf{C}\dot{\mathbf{q}}_w + \mathbf{K}_p\varepsilon_w + \mathbf{K}_d\dot{\varepsilon}_w \\ &\quad + \mathbf{J}_u^{\mathrm{T}}\mathbf{u}_c) + \varepsilon_w^{\mathrm{T}}\mathbf{K}_p\dot{\varepsilon}_w \end{aligned} \tag{30}$$

Note that the formulation in Eq.(22) still preserves the multibody property of $\mathbf{M}$ and $\mathbf{C}$. Therefore, $\dot{\mathbf{M}} - 2\mathbf{C}$ is a skew matrix, resulting in $\dot{\varepsilon}_w^{\mathrm{T}}(\dot{\mathbf{M}} - 2\mathbf{C})\dot{\varepsilon}_w = 0$ [21]. By having $\mathbf{u}_c = \mathbf{J}_u^{-\mathrm{T}}(\mathbf{M}\ddot{\rho} - \mathbf{C}\dot{\rho})$, the derivative of V can be calculated as

$$\dot{V} = -\dot{\varepsilon}_w^{\mathrm{T}}(\mathbf{K}_p\varepsilon_w + \mathbf{K}_d\dot{\varepsilon}_w) + \varepsilon_w^{\mathrm{T}}\mathbf{K}_p\dot{\varepsilon}_w = -\dot{\varepsilon}_w^{\mathrm{T}}(\mathbf{K}_d\dot{\varepsilon}_w) <= 0 \tag{31}$$

which reaches zero only when $\varepsilon_w = \mathbf{0}$ (asymptotic stability).

4 Numerical Simulation

This section presents the numerical simulations of the novel wrist joint model. The simulation is carried out in MATLAB [22] as shown in Fig. 5. Based on human body structures [23], the de-

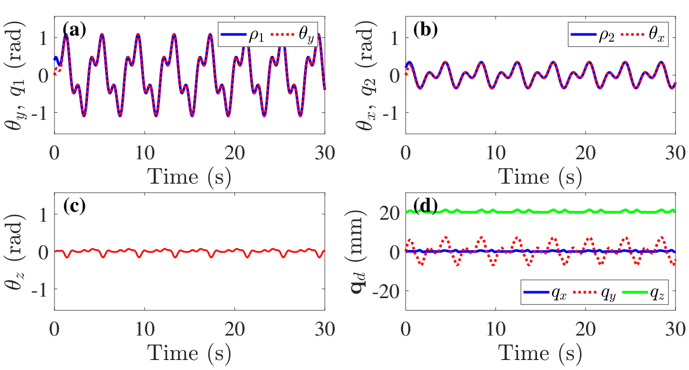

FIGURE 6: The control simulation of the wrist joint model, where (a) and (b) shows the tracking performance of q_1 and q_2, respectively; and (c) and (d) shows the coupled motion of θ_z and $\mathbf{q}_d$, respectively.

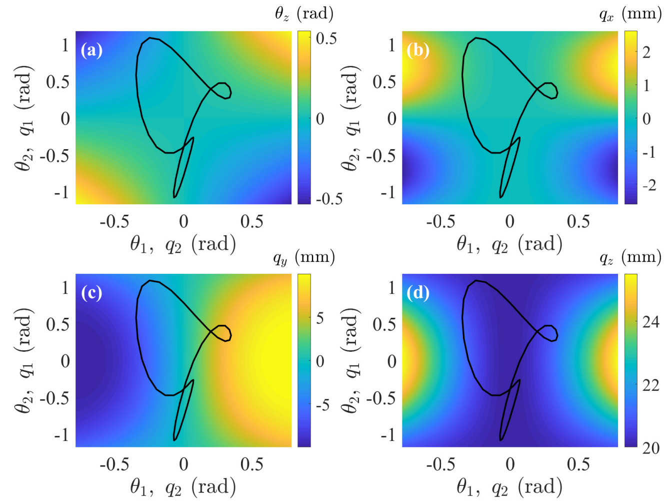

FIGURE 7: Fixed point values of θ_z and $\mathbf{q}_d$, where the red line is the reference trajectory defined in Eq.(33).

fault model and control parameters are selected as

$$\begin{gathered} c_0 = 2\ \text{cm}; \quad k_c = 1.5; \quad l_0 = 10\ \text{cm}; \\ m = 1\ \text{kg}; \quad \phi_0 = 3\times 10^{-3}\ \text{kg}\cdot\text{m}^2; \quad k_s = 0.5; \\ \mathbf{K}_p = \mathbf{I}_2\ \text{N/m}; \quad \mathbf{K}_d = \mathbf{I}_2\ \text{Ns/m} \end{gathered} \tag{32}$$

4.1 Kinematics of the Wrist Joint

In the first simulation, the wrist model is controlled to track the reference trajectory designed as

$$\rho = \frac{\pi}{8}\left[2\sin(\pi t) + \cos(3\pi t)\ \ 0.5\cos(\pi t) - 0.5\sin(2\pi t)\right]^{\mathrm{T}} \tag{33}$$

The result is shown in Fig. 6, which demonstrates that the controller design is valid. It is easy to observe the coupling behavior between the model. While θ_z is not constantly zero, its amplitude is significantly smaller than that of the θ_x (q_2) and θ_y (q_1). The translational displacements of the center of the wrist also varies while the contact point remains on the ellipsoidal surface.

The maps of the fixed point values of θ_z and $\mathbf{q}_d$ calculated from Eq.(28) is shown in Fig. 7. These maps are also the kinematics solutions of the system based on $\mathbf{q}_w$. Notice that as a result of the model parameter selections, Fig. 7(c) and 7(d) are symmetric, while the signs of the values in Fig. 7(a) and 7(b) are reversed with respect to $\theta_y = q_1 = 0$. The values on the reference trajectory of θ_x and θ_y match with the above control simulation results.

4.2 Comparison with Other Wrist Models

The previously used wrist joints mentioned in Section 2 are also modeled for comparison with the proposed model. Here, the rotation constraint $r_{z_\theta,1}$, $r_{z_\theta,2}$, and $r_{z_\theta,3}$ are adopted and tested, while translational constraints $r_{1,d}$ and $r_{2,d}$ are preserved. It should be noted that a conversion is made so that

$$\mathbf{R}_w(\mathbf{z}_\psi) = \mathbf{R}_z(\psi_z)\mathbf{R}_x(\psi_x)\mathbf{R}_y(\psi_y) \tag{34}$$

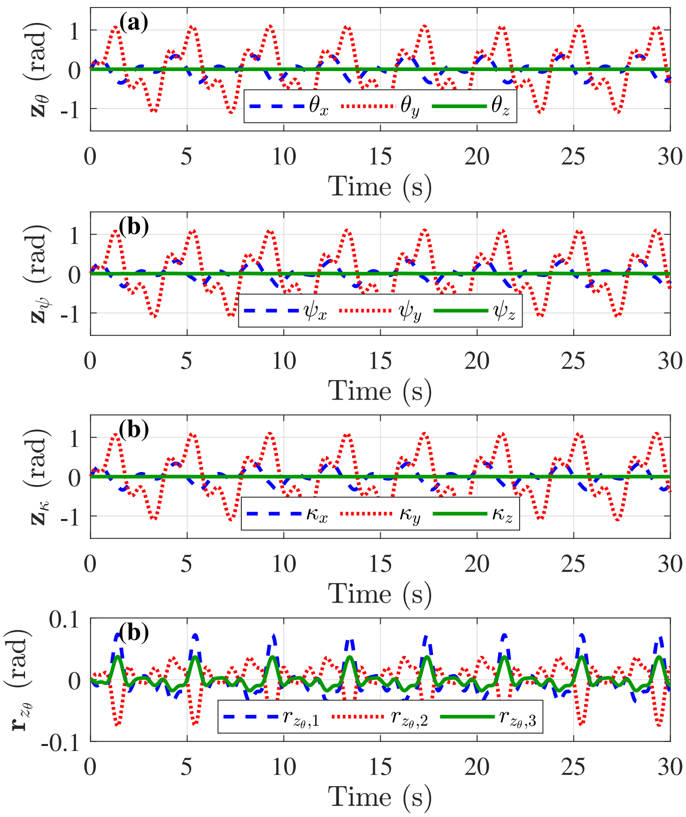

FIGURE 8: The comparison between quaternion based constraints, where (a), (b), and (c) shows the effect of $r_{z_\theta,1}$, $r_{z_\theta,2}$, and $r_{z_\theta,3}$, respectively; and (d) compares the trajectories of r_{z_θ} from the three cases.

where $\mathbf{z}_\psi = \begin{bmatrix}\psi_x, & \psi_y, & \psi_z\end{bmatrix}^{\mathrm{T}}$ is the *z*-*x*-*y* Euler Angle. The constraint $r_{\mathbf{z}_\theta,2}$ is rewritten as

$$r_{\mathbf{z}_\theta,2}(\mathbf{z}_\theta, \mathbf{z}_\psi) = r_{\mathbf{z}_\theta} + \sin(\psi_y/2)\sin(\psi_x/2) = 0 \tag{35}$$

so that $\mathbf{q}_w$ remain as $\mathbf{q}_w = [\theta_y, \ \theta_x]^{\mathrm{T}}$. Similarly, for $r_{z_\theta,3}$, it is converted to

$$\mathbf{R}_w(\mathbf{z}_\theta) = \mathbf{R}_w(\mathbf{z}_\kappa/2)\mathbf{R}_w(\mathbf{z}_\kappa/2) \tag{36}$$

where $\mathbf{z}_\kappa = \begin{bmatrix}\kappa_x, & \kappa_y, & \kappa_z\end{bmatrix}^{\mathrm{T}}$ so that $r_{\mathbf{z}_\theta,3}$ is rewritten as

$$r_{\mathbf{z}_\theta,3}(\mathbf{z}_\theta, \mathbf{z}_\kappa) = r_{\mathbf{z}_\theta} - \sin(\kappa_y/2)\sin(\kappa_x/2)/2 = 0 \tag{37}$$

These constraints are modified based on r_{z_θ} to model the universal joints. The constraints are designed to fix θ_z, ψ_z, and κ_z as zero. The result is shown in Fig. 8, where it is clearly shown that the quaternion based constraints can be used to successfully model the universal joint models, since the rotation angle around *z* in Fig. 8(a-c) are constantly zero. Figure 8(d) presents the trajectories of the original constraint function r_{z_θ} in the three cases, which corroborate the observation in Section 2.1. Hence, the quaternion based constraint function r_{z_θ} is a suitable function basis for the structural identification of the wrist joint in practice.

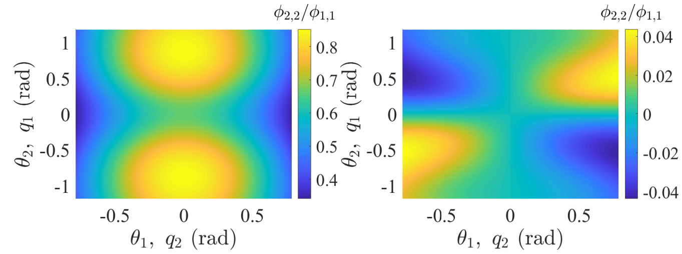

FIGURE 9: The map of ratio between elements of $\mathbf{M}$ with respect to the $\mathbf{q}_w$.

4.3 Nonlinear Dynamical Behaviors

A significantly coupling effect between $\mathbf{q}_w$ is introduced by the inertia matrix. Here, the elements of the inertia matrix $\mathbf{M}$ are explicitly defined as

$$\mathbf{M} = \begin{bmatrix}\phi_{1,1} & \phi_{1,2} \\ \phi_{2,1} & \phi_{2,2}\end{bmatrix} \tag{38}$$

where $\phi_{1,2} = \phi_{2,1}$. As shown in Fig. 9, the element ratios are significantly affected by the change of $\mathbf{q}_w$. The ratio change is especially significant when either q_1 or q_2 is large. This nonlinearity can significantly affect the system dynamics during high frequency or large range motions.

If $\mathbf{K}_p$ or $\mathbf{K}_d$ are not positive definite, the unstable fixed points may result in periodic or chaotic solutions. To showcase such system behaviors, $\mathbf{u}_c$ is designed as

$$\mathbf{u}_c = \mathbf{K}_{p,3}\varepsilon^3 + \mathbf{K}_{d,3}\dot{\varepsilon}^3 \tag{39}$$

where $\mathbf{K}_{p,3}$ and $\mathbf{K}_{d,3}$ are cubic stiffness and damping. Therefore, by adding a small perturbation in $\dot{\mathbf{q}}_w$, under different parameters, the system demonstrates periodic and chaotic-like solutions, whose examples are as shown in Fig. 10. The cause of these solutions can be investigated through parametric studies, which will provide insights into how self-excited mechanical or neural-feedback oscillations may occur in human body due to physiological and pathological tremors [24, 25].

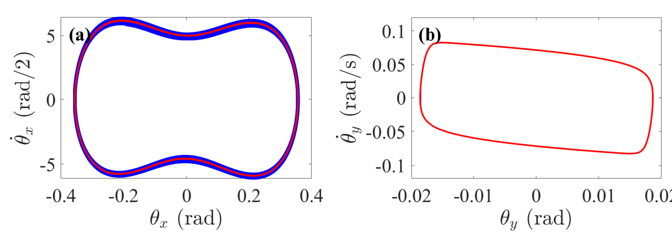

FIGURE 10: The phase portraits of the system, where a chaotic-like solution is shown (a) and a limit cycle solution is shown in (b) [24, 25]. The red dot line is shows the last 5% of the trajectory. For (a), the control gaines are selected as: $\mathbf{K}_p = -3\mathbf{I}_2$. $\mathbf{K}_d = 10^{-3}\mathbf{I}_2$, $\mathbf{K}_{p,3} = 100\mathbf{I}_2$, $\mathbf{K}_{d,3} = \mathbf{0}_{2\times2}$; and for (b), the control gaines are selected as: $\mathbf{K}_p = \mathbf{I}_2$. $\mathbf{K}_d = -0.5\mathbf{I}_2$, $\mathbf{K}_{p,3} = \mathbf{0}_{2\times2}$, $\mathbf{K}_{d,3} = 100\mathbf{I}_2$.

5 Conclusion and Future Work

This paper presented a novel ellipsoidal joint to model wrist kinematics. Unlike the previous wrist joints modeled as universal joints, the proposed model was designed based on quaternion-based rotation constraints and ellipsoid-contact-based translational constraints. Dynamical modeling was carried out to obtain a minimal-order state-space model. The equilibrium and stability of the wrist joint were analyzed, leading to the design of an asymptotically stable controller. The simulation of the wrist dynamics validated the analytical results. The comparison with the universal joints also showed that the proposed wrist joint model is an ideal candidate for identifying and regressing the true kinematic structure of the wrist. Finally, with the involvement of negative and nonlinear stiffness/damping, the chaotic and periodic nonlinear solutions were discovered.

The proposed ellipsoidal joint is a generalized model, which can be used for future studies. The continuation of this work will include the nonlinear and bifurcation analysis of the wrist dynamics. The ellipsoidal wrist model will also be used in the kinematic identification of the true wrist joint, as well as the design of better upper limb rehabilitation devices [6].

REFERENCES

[1] Maciejasz, P., Eschweiler, J., Gerlach-Hahn, K., Jansen-Troy, A., and Leonhardt, S., 2014. "A survey on robotic devices for upper limb rehabilitation". *Journal of neuroengineering and rehabilitation,* ***11***(1), p. 3.

[2] Gupta, A., O'Malley, M. K., Patoglu, V., and Burgar, C., 2008. "Design, control and performance of ricewrist: a force feedback wrist exoskeleton for rehabilitation and training". *The International Journal of Robotics Research,* ***27***(2), pp. 233–251.

[3] Pezent, E., Rose, C. G., Deshpande, A. D., and O'Malley, M. K., 2017. "Design and characterization of the openwrist: A robotic wrist exoskeleton for coordinated hand-wrist rehabilitation". In 2017 International Conference on Rehabilitation Robotics (ICORR), IEEE, pp. 720–725.

[4] Loureiro, R. C., Belda-Lois, J. M., Lima, E. R., Pons, J. L., Sanchez-Lacuesta, J. J., and Harwin, W. S., 2005. "Upper limb tremor suppression in adl via an orthosis incorporating a controllable double viscous beam actuator". In 9th International Conference on Rehabilitation Robotics, 2005. ICORR 2005., Ieee, pp. 119–122.

[5] Taheri, B., 2013. "Real-time pathological tremor identification and suppression in human arm via active orthotic devices". PhD thesis, Southern Methodist University.

[6] Wang, J., Barry, O., Kurdila, A. J., and Vijayan, S., 2019. "On the dynamics and control of a full wrist exoskeleton for tremor alleviation". In ASME 2019 Dynamic Systems and Control Conference, American Society of Mechanical Engineers Digital Collection.

[7] Wang, J., and Barry, O. "Multibody analysis and control of a full-wrist exoskeleton for tremor alleviation". *Journal of Biomechanical Engineering*.

[8] Moore, D. C., Crisco, J. J., Trafton, T. G., and Leventhal, E. L., 2007. "A digital database of wrist bone anatomy and carpal kinematics". *Journal of biomechanics,* ***40***(11), pp. 2537–2542.

[9] Akhbari, B., Moore, D. C., Laidlaw, D. H., Weiss, A.-P. C., Akelman, E., Wolfe, S. W., and Crisco, J. J., 2019. "Predicting carpal bone kinematics using an expanded digital database of wrist carpal bone anatomy and kinematics". *Journal of Orthopaedic Research®*.

[10] Salvia, P., Woestyn, L., David, J. H., Feipel, V., Van, S., Jan, S., Klein, P., and Rooze, M., 2000. "Analysis of helical axes, pivot and envelope in active wrist circumduction". *Clinical Biomechanics,* ***15***(2), pp. 103–111.

[11] Li, Z.-M., Kuxhaus, L., Fisk, J. A., and Christophel, T. H., 2005. "Coupling between wrist flexion-extension and radial-ulnar deviation". *Clinical biomechanics,* ***20***(2), pp. 177–183.

[12] Formica, D., Charles, S. K., Zollo, L., Guglielmelli, E., Hogan, N., and Krebs, H. I., 2012. "The passive stiffness of the wrist and forearm". *Journal of neurophysiology,* ***108***(4), pp. 1158–1166.

[13] Drake, W. B., and Charles, S. K., 2014. "Passive stiffness of coupled wrist and forearm rotations". *Annals of biomedical engineering,* ***42***(9), pp. 1853–1866.

[14] Duprey, S., Naaim, A., Moissenet, F., Begon, M., and Cheze, L., 2017. "Kinematic models of the upper limb joints for multibody kinematics optimisation: An overview". *Journal of biomechanics,* ***62***, pp. 87–94.

[15] Seth, A., Hicks, J. L., Uchida, T. K., Habib, A., Dembia, C. L., Dunne, J. J., Ong, C. F., DeMers, M. S., Rajagopal, A., Millard, M., et al., 2018. "Opensim: Simulating musculoskeletal dynamics and neuromuscular control to study human and animal movement". *PLoS computational biology,* ***14***(7), p. e1006223.

[16] Yu, N., and Xu, C., 2020. "An improved wrist kinematic model for human-robot interaction". *arXiv preprint arXiv:2002.05790*.

[17] Seth, A., Sherman, M., Eastman, P., and Delp, S., 2010. "Minimal formulation of joint motion for biomechanisms". *Nonlinear dynamics,* ***62***(1-2), pp. 291–303.

[18] Biryukova, E., Roby-Brami, A., Frolov, A., and Mokhtari, M., 2000. "Kinematics of human arm reconstructed from spatial tracking system recordings". *Journal of biomechanics,* ***33***(8), pp. 985–995.

[19] Rose, C. G., Pezent, E., Kann, C. K., Deshpande, A. D., and O'Malley, M. K., 2018. "Assessing wrist movement with robotic devices". *IEEE Transactions on Neural Systems and Rehabilitation Engineering,* ***26***(8), pp. 1585–1595.

[20] Crisco, J. J., Heard, W. M., Rich, R. R., Paller, D. J., and Wolfe, S. W., 2011. "The mechanical axes of the wrist are

oriented obliquely to the anatomical axes". *The Journal of Bone and Joint Surgery. American volume.,* ***93***(2), p. 169.

[21] Khalil, H. K., and Grizzle, J. W., 2002. *Nonlinear systems*, Vol. 3. Prentice hall Upper Saddle River, NJ.

[22] Wang, J., Kamidi, V. R., and Ben-Tzvi, P. "A multibody toolbox for hybrid dynamic system modeling based on nonholonomic symbolic formalism". In ASME 2018 Dynamic Systems and Control Conference, American Society of Mechanical Engineers Digital Collection.

[23] Clauser, C. E., McConville, J. T., and Young, J. W., 1969. Weight, volume, and center of mass of segments of the human body. Tech. rep., Antioch Coll Yellow Springs OH.

[24] Palanthandalam-Madapusi, H. J., and Goyal, S., 2011. "Is parkinsonian tremor a limit cycle?". *Journal of Mechanics in Medicine and Biology,* ***11***(05), pp. 1017–1023.

[25] Timmer, J., Häußler, S., Lauk, M., and Lücking, C.-H., 2000. "Pathological tremors: Deterministic chaos or nonlinear stochastic oscillators?". *Chaos: An Interdisciplinary Journal of Nonlinear Science,* ***10***(1), pp. 278–288.